# Molecular orbital studies, frequency and solvent dependent NLO properties of (2E)-1-(4-bromophenyl)-3-(4-nitrophenyl) prop-2-en-1-one

K Anitha[a], V Balachandran[b]* & B Narayana[c]

[a]Department of Physics, Bharathidasan University Constituent College, Lalgudi, Tiruchirapalli 621 601, India

[b]Centre for Research, Department of Physics, A A Government Arts College, Musiri, Tiruchirapalli 621 211, India

[c]Department of Studies in Chemistry, Mangalore University, Mangalagangotri 574 199, India

FTIR and FT-Raman spectrum of (2E)-1-(4-bromophenyl)-3-(4-nitrophenyl) prop-2-en-1-one (BP4NP) have been recorded in the region $4000-400$ cm$^{-1}$ and $4000-50$ cm$^{-1}$, respectively. The structural and spectroscopic data of the molecule in the ground state have been calculated by using B3LYP/6-31+G (d) and CAM-B3LYP/ 6-31+G (d) basis sets. The vibrational frequencies have been calculated and compared with the experimental frequencies, which yield good agreement between observed and calculated frequencies. NBO analysis has been performed in order to demonstrate charge transfer or conjugative interaction and delocalization of electron density within the molecule. The electronic absorption spectra have been investigated by the TD-DFT methods. Besides, the highest occupied molecular orbital energy (HOMO), the lowest unoccupied molecular orbital energy (LUMO) and energy difference (HOMO–LUMO) between the frontier molecular orbitals, reactive descriptors and molecular electrostatic potential (MEP) have been performed. The static and dynamic (frequency) average polarizability (α), first- and second- order hyperpolarizabilities (β and γ) have been investigated by using the CAM-B3LYP method. The solvent effects on the polarizability (α), first- and second- order hyperpolarizabilities (β and γ) have also been evaluated by IEFPCM model. The results display significant second- and third-order molecular nonlinearity of the title compound.

**Keywords:** Vibrational spectra, HOMO-LUMO, NBO analysis, Static NLO, Dynamic NLO

## 1 Introduction

Organic molecules with significant nonlinear optical activity generally consist of a π-electron conjugated moiety substituted by an electron donor group on one end of the conjugated structure and an electron acceptor group on the other end, forming a "push-pull" conjugated structure[1-3]. In general, the second order NLO chromophore can be divided into three blocks; an electro-donor, a π -conjugated bridge and a strong electro acceptor, called the D–π–A system. When under an applied external electric field, the donor and acceptor substituents can provide the requisite ground-state charge asymmetry, whereas the π-conjugation bridge provides a pathway for the ultrafast redistribution of electric charges[4]. The extent of the redistribution is measured by dipole moment, the linear response into an applied field by the (linear) polarizability (α) and the asymmetry of this redistribution with respect to the polarity of the field by the first-order hyperpolarizability (β). The photophysical properties of these π-conjugated compounds originate mainly from the intra-molecular

charge transfer state that depends strongly on the substituent effect and properties of solvents. The electron acceptor group in a π-conjugated organic molecule withdraws electronic charge from the electron donor group through the conjugated bridge, resulting in the polarization of the π-electron skeleton. The photophysical properties of this class of organic compounds originate mainly from the donor-acceptor interaction and high level of the π-conjugated charge transfer. Hence, conjugated organic compounds are good candidates to a great extent, as it can be tuned and tailored by structural modification for their potential applications in organic optoelectronic devices such as organic field-effect transistors (OFET), organic light emitting diodes (OLEDs), and other all optical devices[3]. Chalcones are a class of compounds in which two aromatic planar rings are connected through α, β-unsaturated carbonyl system with strong electron donor-acceptor interactions depending on the substituent attached to the aromatic rings. Apart from very important biological and pharmaceutical applications, the photophysical properties of chalcones have attracted considerable research attention including metal sensing, optical materials, laser dyes, etc[5-7].

_____

*Corresponding author (E-mail: brsbala@rediffmail.com)

## 2 Experimental Details

A solution of potassium hydroxide (5%, 5 mL) was added slowly with stirring to a mixture of 4-nitrobenzaldehyde (1.51 g, 0.01 mol) and 4- bromoacetophenone (1.99 g, 0.01 mol) in ethanol (30 mL). The mixture was stirred at room temperature for 24 h. The precipitated solid was filtered, washed with water, dried and crystals of (I) were recrystallized from acetone by slow evaporation (yield; 68%; m.p. 439–441 K). Analysis found (calculated) for $C_{15}H_{10}BrNO_3$ (%); C 54.11 (54.24), H 3.04 (3.03), N 4.10 (4.22)[8]. The Perkin Elmer Spectrum FTIR instrument consists of globar and mercury vapor lamp as sources, an interferometer chamber comprising of KBr and mylar beam splitters followed by a sample chamber and detector. The entire region of 400-4000 $cm^{-1}$ is covered by this instrument. The spectrometer works under purged conditions. Solid samples are dispersed in KBr or polyethylene pellets depending on the region of interest. This instrument has a typical resolution of 1.0 $cm^{-1}$. Signal averaging, signal enhancement, base line correction and other spectral manipulations are possible. The FT-Raman spectrum of the BP4NP was also recorded in FT-Raman BRUKER RFS 100/S instrument equipped with Nd:YAG laser source operating at 1064 nm wavelength and 150 mW power. The spectrum is recorded in the range 4000–50 $cm^{-1}$. The spectral resolution is 2 $cm^{-1}$.

## 3 Computational Details

Calculations of the title compound are carried out with Gaussian09 program[9] using the B3LYP/6-31+G (d) and CAM-B3LYP/ 6-31+G (d) basis sets to predict the molecular structure and vibrational wavenumbers. Molecular geometry was fully optimized for the calculations of vibrational frequencies, infrared intensities, and Raman activities. The hybrid functional method tends to overestimate the fundamental modes; therefore scaling factor of 0.9613 has to be used for obtaining a considerably better agreement with experimental data. The assignments of the calculated wavenumbers are aided by the animation option of GAUSSVIEW[10] program, which gives a visual presentation of the vibrational modes. The vibrational modes are assigned on the basis of potential energy distribution (PED) analysis using vibrational energy distribution analysis (VEDA) program[11]. The natural bond orbital (NBO) analysis were performed on BP4NP by the NBO 3.1 program[12] at the B3LYP/6-31+G (d) level as implemented in the Gaussian 09W software package[9]. These calculations yielded second-order perturbation energies which have been utilized in locating hydrogen bonding and hyperconjugative interactions.

From the basic theory of Raman scattering, Raman activities ($s_i$) calculated by Gaussian 09 program have been converted to relative Raman intensities ($I_i$) using the following relationship[13]:

$$I_i = \frac{f(\upsilon_0 - \upsilon_i)^4 s_i}{\upsilon_i [1 - \exp(-hc\upsilon_i)]/kT}$$

where $\upsilon_0$ is the laser exciting wavenumber in $cm^{-1}$ (in this work, we have used the excitation wavenumber $\upsilon_0$ =9398.5 $cm^{-1}$, which corresponds to the wavelength of 1064 nm of Nd:YAG laser), $\upsilon_i$ is the vibrational wavenumber of the $i^{th}$ normal mode in $cm^{-1}$, $h, c,$ and $k$ are universal constants (is a constant equal to $10^{-12}$) and $f$ is a suitably chosen common normalization factor for all the peak intensities.

## 4 NLO Theory

In nonlinear optics, calculation of hyperpolarizability is achieved via the finite field method. The energy ($E$) of a molecule in presence of a static homogeneous electric field ($F$) can be expanded as follows:

$$E(F) = E(0) - \mu_i F_i - \frac{1}{2}\alpha_{ij}F_iF_j - \frac{1}{6}\beta_{ijk}F_iF_jF_k - \frac{1}{24}\gamma_{ijkl}F_iF_jF_kF_l$$

where $\alpha_{ij}$, $\beta_{ijk}$ and $\gamma_{ijkl}$ are the polarizability, the first hyperpolarizability and second hyperpolarizability tensors, respectively. The subscripts $i, j$ and $k$ represent $x, y$ and $z$ Cartesian co-ordinate system. $E(0)$ is the energy of the compound in the absence of $\vec{F}$, $\mu_i$ is the molecular permanent electric dipole moment along the $i^{th}$ direction, $F_i$ is the $i^{th}$ component of $\vec{F}$. In dynamic electric fields, $\alpha_{ij}$, $\beta_{ijk}$ and $\gamma_{ijkl}$ are frequency-dependent and related to different optical responses[14]. In this study, the average linear polarizability $\alpha$ and second hyperpolarizability $\beta$ values have been calculated using the following expressions, respectively:

$$\alpha = \frac{\alpha_{xx} + \alpha_{yy} + \alpha_{zz}}{3}$$

The static first hyperpolarizability $\beta$ was calculated by analytical third energy derivatives, which is more

efficient and less expensive. The total first-order polarizabilities ($\beta_{tot}$) for the studied complexes are defined as:

$$\beta = \left( \beta_x^2 + \beta_y^2 + \beta_z^2 \right)^{1/2}$$

where $\beta_i$ is defined as:

$$\beta_i = \left( \beta_{iii} + \beta_{ijj} + \beta_{ikk} \right) \ i, j, k = x, y, z.$$

The average second hyperpolarizability $\gamma_{ijkl}$ can be directly calculated from Gaussian 09[9]. The equation for average second hyperpolarizability is:

$$\langle \gamma \rangle = \frac{1}{5} \left[ \gamma_{xxxx} + \gamma_{yyyy} + \gamma_{zzzz} + 2 \left( \gamma_{xxyy} + \gamma_{xxzz} + \gamma_{yyzz} \right) \right]$$

The tensor elements parallel to long molecular axes or parallel to large transition dipole moments dominate the isotropic values $\overline{\gamma}$. The components of linear polarizability, first and second hyperpolarizabilities of the title compound is computed. Since the values of the polarizabilities $\alpha$, first hyperpolarizability $\beta$ and second hyperpolarizability $\gamma$ of Gaussian 09 output are reported in atomic units (a.u.), the calculated values have been converted into electrostatic units (esu) ($\alpha$: 1 a.u = $0.1482 \times 10^{-24}$ e.s.u; $\beta$: 1 a.u = $8.6393 \times 10^{-33}$ e.s.u and $\gamma$ : 1 a.u = $5.0367 \times 10^{-40}$ e.s.u).

To check the consistency of the calculation, $\beta$ and $\gamma$ values were calculated using long-range corrected (CAM-B3LYP) functional[15] at 6−31+G (d) basis set level. Furthermore, to understand the influence of the dispersion (frequency dependence) and the effect of the electron correlation on the NLO properties, the frequency-dependent ($\beta$ and $\gamma$) of BP4NP was evaluated using couple-perturbed (CP) DFT method

with CAM-B3LYP functional. In addition, the IEFPCM (integral equation formulation polarisable continuum model) has been used to examine the solvent effect on the static and dynamic polarizability ($\alpha$), first order ($\beta$) and second order ($\gamma$) hyperpolarizability of this compound. To further explain the second- and third- order NLO behaviour for the title compound, we employed time-dependent density functional theory (TD-DFT) methods to descript their electronic spectra. To choose suitable calculated methods, the electron absorption spectra of BP4NP was simulated using TD-DFT and CAM-B3LYP method with the basis set 6-31+G (d) level in gas phase and in IEFPCM in different solvent solution.

## 5 Results and Discussion

### 5.1 Structural properties

The molecular structure and numbering of the atoms of BP4NP are shown in Fig. 1. The optimized geometrical parameters of BP4NP obtained by DFT/B3LYP and LC-DFT/CAM-B3LYP with 6-31+G (d) basis set are presented in Table 1.

In the present work, geometry optimization parameters for BP4NP have been employed without symmetry constrain. From Table 1, it is found that the bond lengths and bond angles calculated by DFT/B3LYP and CAM-B3LYP methods are consistent with experimental values[8]. Optimization of properties of non-linear optical materials involves molecular design by considering different classes of chromophores and factors able to affect (and enhance) the internal charge transfer interaction, such as substitution of the electron acceptor/donor groups on phenylene and benzoyl moieties of chalcone which significantly alters the $\beta$ values[16]. In the molecular structure of BP4NP crystal, the para position of
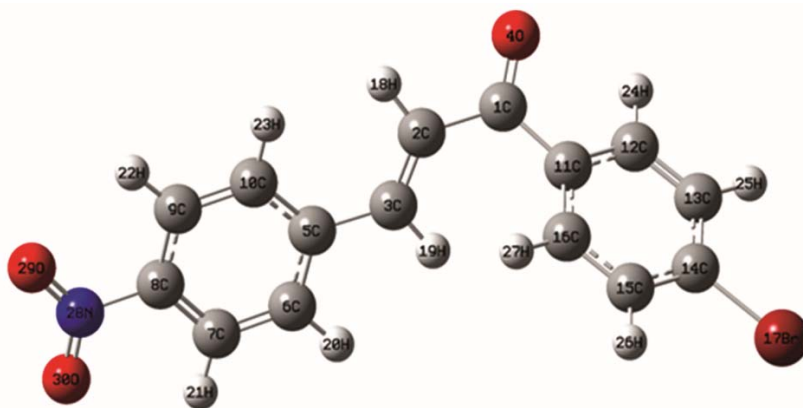


Fig. 1 — Optimised geometry of (2E)-1-(4-bromophenyl)-3-(4-nitrophenyl) prop-2-en-1-one.

Table 1 — A comparison between the optimized geometrical parameters calculated at B3LYP and the long range corrected DFT functional CAM-B3LYP at 6-31+G (d) level of theory for (2E)-1-(4-bromophenyl)-3-(4-nitrophenyl)prop-2-en-1-one.

| Bond length (Å) | | | Bond angle (°) | | | Dihedral angle (°) | | |
|---|---|---|---|---|---|---|---|---|
| | Calculated values | | | Calculated values | | | Calculated values | |
| Parameter | Experimental values[a] | B3LYP/ 6-31+G (d) | CAM-B3LYP/ 6-31+G (d) | Parameter | Experimental values[a] | B3LYP/ 6-31+G (d) | CAM-B3LYP/ 6-31+G (d) | Parameter | Experimental values[a] | B3LYP/ 6-31+G (d) | CAM-B3LYP/ 6-31+G (d) |
| C1−C2 | 1.48 | 1.49 | 1.49 | C2−C1−O4 | 121.41 | 118.33 | 118.52 | C2−C1−C11−C12 | -171.99 | 153.12 | 153.15 |
| C1−O4 | 1.22 | 1.23 | 1.22 | O4−C1−C11 | 119.90 | 120.20 | 120.13 | O4−C1−C11−C16 | -169.06 | 150.49 | 150.73 |
| C1−C11 | 1.50 | 1.50 | 1.50 | C3−C2−H18 | 118.97 | 121.35 | 121.65 | C1−C2−C3−C5 | 177.37 | -173.55 | -173.81 |
| C2−C3 | 1.33 | 1.35 | 1.34 | C2−C3−C5 | 126.02 | 126.88 | 126.55 | H18−C2−C3−C5 | -2.71 | -2.63 | -2.60 |
| C2−H18 | 0.95 | 1.09 | 1.09 | C2−C3−H19 | 117.02 | 118.40 | 118.63 | H18−C2−C3−H19 | 177.26 | 175.65 | 175.57 |
| C3−C5 | 1.47 | 1.47 | 1.47 | C3−C5−C10 | 119.14 | 123.24 | 122.93 | H19−C3−C5−C6 | 170.73 | -1.73 | -4.67 |
| C3−H19 | 0.95 | 1.09 | 1.09 | C6−C5−C10 | 118.51 | 118.31 | 118.60 | C3−C5−C6−C7 | -179.04 | 179.86 | -179.95 |
| C5−C6 | 1.40 | 1.41 | 1.40 | C5−C6−H20 | 119.44 | 119.28 | 119.35 | C3−C5−C6−H20 | 0.89 | -0.30 | -0.19 |
| C5−C10 | 1.40 | 1.41 | 1.40 | C6−C7−C8 | 118.52 | 118.52 | 118.38 | C10−C5−C6−C7 | -0.56 | 0.14 | 0.36 |
| C6−C7 | 1.38 | 1.39 | 1.39 | C7−C8−C9 | 122.75 | 121.84 | 122.10 | C10−C5−C6−H20 | 179.37 | 179.98 | -179.88 |
| C6−H20 | 0.95 | 1.09 | 1.09 | C7−C8−N28 | 118.61 | 119.08 | 118.96 | C3−C5−C10−C9 | 178.82 | -179.81 | -179.97 |
| C7−C8 | 1.38 | 1.39 | 1.39 | C9−C8−N28 | 118.62 | 119.07 | 118.94 | C6−C5−C10−H23 | -179.79 | 179.79 | 179.41 |
| C7−H21 | 0.95 | 1.08 | 1.08 | C8−C9−C10 | 117.99 | 118.93 | 118.76 | C5−C6−C7−C8 | 0.51 | -0.09 | -0.20 |
| C8−C9 | 1.38 | 1.40 | 1.39 | C5−C10−C9 | 121.15 | 121.00 | 120.89 | C5−C6−C7−H21 | -179.43 | 179.93 | 179.84 |
| C8−N28 | 1.48 | 1.47 | 1.47 | C1−C11−C12 | 118.25 | 117.68 | 117.51 | H20−C6−C7−C8 | -179.43 | -179.93 | -179.96 |
| C9−C10 | 1.39 | 1.39 | 1.38 | C1−C11−C16 | 123.20 | 123.30 | 123.26 | C6−C7−C8−N28 | 177.97 | -179.93 | -179.89 |
| C9−H22 | 0.95 | 1.08 | 1.08 | C12−C11−C16 | 118.52 | 118.92 | 119.14 | H21−C7−C8−C9 | 179.76 | 179.98 | 179.93 |
| C10−H23 | 0.95 | 1.08 | 1.08 | C11−C12−C13 | 121.40 | 120.91 | 120.78 | C7−C8−C9−H22 | 179.84 | -179.93 | -179.79 |
| C11−C12 | 1.40 | 1.40 | 1.40 | C11−C12−H24 | 119.38 | 118.61 | 118.59 | N28−C8−C9−C10 | 178.23 | 179.96 | 179.95 |
| C11−C16 | 1.40 | 1.40 | 1.40 | C13−C12−H24 | 119.22 | 120.48 | 120.63 | C7−C8−N28−O29 | -176.20 | 180.00 | -179.99 |
| C12−C13 | 1.38 | 1.39 | 1.39 | C12−C13−C14 | 118.62 | 119.04 | 119.09 | C9−C8−N28−O30 | -177.88 | -179.92 | -179.85 |
| C12−H24 | 0.95 | 1.09 | 1.08 | C12−C13−H25 | 120.64 | 120.83 | 120.87 | C8−C9−C10−H23 | -179.90 | -179.87 | -179.63 |
| C13−C14 | 1.40 | 1.40 | 1.39 | C13−C14−C15 | 121.32 | 121.26 | 121.19 | H22−C9−C10−C5 | -179.90 | 179.98 | 179.96 |
| C13−H25 | 0.95 | 1.08 | 1.08 | C13−C14−Br17 | 120.11 | 119.36 | 119.40 | C1−C11−C12−C13 | -176.70 | 178.22 | 178.32 |
| C14−C15 | 1.38 | 1.39 | 1.39 | C15−C14−Br17 | 118.51 | 119.38 | 119.40 | C16−C11−C12−C13 | 1.50 | 1.79 | 1.74 |
| C14−Br17 | 1.90 | 1.91 | 1.89 | C14−C15−C16 | 119.65 | 119.12 | 119.19 | C16−C11−C12−H24 | -178.57 | -178.19 | -178.13 |
| C15−C16 | 1.39 | 1.39 | 1.39 | C11−C16−C15 | 120.47 | 120.73 | 120.58 | C1−C11−C16−C15 | 176.36 | -177.09 | -177.26 |
| C15−H26 | 0.95 | 1.08 | 1.08 | C8−N28−O29 | 118.32 | 117.61 | 117.59 | C12−C11−C16−H27 | 178.23 | 177.15 | 177.36 |
| C16−H27 | 0.95 | 1.09 | 1.08 | C8−N28−O30 | 117.67 | 117.61 | 117.59 | C11−C12−C13−H25 | 179.82 | 179.07 | 179.16 |
| N28−O29 | 1.23 | 1.23 | 1.22 | O29−N28−O30 | 124.01 | 124.78 | 124.82 | H24−C12−C13−C14 | 179.80 | 178.67 | 178.64 |
| N28−O30 | 1.23 | 1.23 | 1.22 | | | | | C12−C13−C14−Br17 | 179.10 | -179.70 | -179.76 |
| | | | | | | | | Br17−C14−C15−C16 | -179.38 | -179.41 | -179.41 |
| | | | | | | | | Br17−C14−C15−H26 | 0.66 | 0.97 | 0.91 |

[a]Ref[8]

chalcone ring consists of a Br atom. Br acts as electron donor and $NO_2$ as strong electron acceptor group. BP4NP containing Br and $NO_2$ at the ends and an electron acceptor C=O at the middle forms a D-π-A-π-A (an effective D-π-A) system, where effective charge transfer takes place from donor end to the acceptor end of the molecule. The donor/acceptor group substituted on the benzoyl and phenyl ring greatly alters the molecular hyperpolarizability of the chalcone derivatives.

### 5.2 Vibrational spectral analysis

Modern vibrational spectrometry has proven to be an exceptionally powerful technique for solving many chemical problems. It has been extensively employed both in the study of chemical kinetics and chemical analysis. The total number of atoms in BP4NP is 30; therefore there are 84 (3N-6) normal modes. The optimized structural parameters have been evaluated for the calculations of vibrational frequencies. It is generally accepted that the geometric parameters depend upon the method and the basis set used in the calculations. The molecular structure optimization of BP4NP and corresponding vibrational harmonic frequencies are calculated at DFT/B3LYP and CAM-B3LYP levels combined with standard 6-31+G(d) basis set to aid interpretation of experimental spectroscopic data. At the optimized geometry for the title molecule no imaginary frequency modes were obtained. The general significance of the obtained results is to improve our understanding of the dynamics of NLO material BP4NP. The calculated vibrational wavenumbers, measured FTIR and FT-Raman band positions and the calculated PED for each normal mode are given in Table 2. The experimental and theoretically predicted FTIR spectra in the region 4000–400 cm$^{-1}$ and the corresponding FT-Raman spectra in the region 4000–50 cm$^{-1}$ are given in Figs 2 and 3, respectively.

BP4NP shows the presence of C−H stretching vibrations in the region of 3100 – 3000 cm$^{-1}$, which is the characteristic region for C−H stretching vibrations[16]. These vibrations usually appear with strong Raman intensity and are highly polarized. In this region, the bands are not affected appreciably by the nature and position of the substituent. The C−H stretching vibrations are observed at 3108, 3093, 3079, 3062, 3043 cm$^{-1}$ (in FTIR) and 3084, 3068, 3028 cm$^{-1}$ (in FT-Raman), and their corresponding calculated values 3106, 3093, 3080, 3060, 3042, 3025 cm$^{-1}$ (in B3LYP/6-31+G (d)) and 3108, 3096, 3087, 3070, 3044, 3029 cm$^{-1}$ (in CAM-B3LYP/6-31+G (d)) are

quite compatible. The C−H in-plane bending vibration usually occurs in the region 1400–1050 cm$^{-1}$ and the C−H out-of-plane[17] bending vibrations in the range 1000–675 cm$^{-1}$. In our study, the C−H in-plane bending vibrations have been observed at 1412, 1317, 1288, 1215, 1179, 1132 and 1108 cm$^{-1}$ in FTIR and 1412, 1182 and 1108 cm$^{-1}$ in FT- Raman. The computed values at 1414, 1317, 1288, 1216, 1180, 1133, 1110 cm$^{-1}$ (B3LYP/6-31+G (d)) and 1416, 1320, 1285, 1221, 1183, 1138 cm$^{-1}$ (CAM-B3LYP/6-31+G (d)) are in good agreement with the experimental values. For C−H out-of-plane vibrations have been observed at 984, 905, 892, 855, 834, 821 and 789 cm$^{-1}$ in FTIR and 984, 892 and 857 cm$^{-1}$ in FT-Raman and their corresponding calculated values 985, 906, 893, 855, 835, 820, 790 cm$^{-1}$ (in B3LYP/6-31+G (d)) and 982, 900, 895, 858, 830, 822, 792 cm$^{-1}$ (in B3LYP/6-31+G (d)).

The C−C ring stretching vibrations are expected within the region 1650–1200 cm$^{-1}$. In general, the bands of variable intensity are observed at 1625–1590, 1575–1590, 1470–1540, 1430–1465 and 1280–1380 cm$^{-1}$ from the frequency ranges given by Varsanyi[17] for the five bands in the region. Most of the ring modes are altered by the substitution to aromatic ring. The actual positions of these modes are determined not so much by the nature of the substituent but by the form of substitution around the ring system. The C−C stretching vibrations are observed at 1607, 1596, 1584, 1534, 1493, 1396 and 1348cm$^{-1}$ in FTIR and at 1607, 1596, 1584, 1534, 1396, 1293 and 1148 cm$^{-1}$ in FT-Raman spectra. The theoretical computed C−C−C in-plane and out-of-plane bending vibrations by the B3LYP/6-31+G (d) and CAM-B3LYP/6-31+G (d) show good agreement with the recorded spectral data. The other wavenumbers of the ring groups such as; torsional and rocking modes are also assigned, and presented in Table 2. All these calculated values are in good agreement with the experimental data.

Aromatic nitro compounds have strong absorption due to the asymmetric and symmetric stretching vibrations in the range 1625–1510 cm$^{-1}$ and 1400–1360 cm$^{-1}$, respectively[18]. The asymmetric and symmetric stretching vibrations provide an unmistakable identity for the existence of $NO_2$ group in the molecule, not only because of their spectral region but also for their strong intensity[19]. The vibrations at 1485 and 1325 cm$^{-1}$ in FT-Raman have been assigned to asymmetric and symmetric stretching modes of $NO_2$ group. The theoretically computed wavenumbers at 1485 and 1325 cm$^{-1}$ show good correlation with the experimental data.

Table 2 — Comparison of the experimental (FTIR and FT-Raman) wavenumbers (cm⁻¹) and theoretical wavenumbers (cm⁻¹) of (2E)-1-(4-bromophenyl)-3-(4-nitrophenyl) prop-2-en-1-one calculated by B3LYP/6- 31+G (d) and CAM- B3LYP/6- 31+G (d).

| S. No. | Experimental (cm⁻¹) | | Calculated frequencies( cm⁻¹) Scaled | | ᵃPED (%) among types of internal coordinates |
|---|---|---|---|---|---|
| | FTIR | FT-Raman | B3LYP/ 6-31+G(d) | CAM-B3LYP/ 6-31+G(d) | |
| 1 | 3108 | | 3106 | 3108 | $v$C7−H21(98) |
| 2 | 3093 | | 3093 | 3096 | $v$C9−H22(96) |
| 3 | | 3084 | 3085 | 3087 | $v$C12−H24(93) |
| 4 | 3079 | | 3080 | 3085 | $v$C15−H26(72), $v$C13−H25(51), $v$C16−H27(23), |
| 5 | | 3068 | 3071 | 3070 | $v$C10−H23(91) |
| 6 | 3062 | | 3060 | 3061 | $v$C12−H24(52), $v$C13−H25(44) |
| 7 | 3043 | | 3042 | 3044 | $v$C16−H27(74), $v$C15−H26(24), $v$C16−H27(23) |
| 8 | | 3028 | 3025 | 3029 | $v$C6−H20(94) |
| 9 | 2923 | | 2920 | 2925 | $v$C2−H18(90) |
| 10 | 2887 | | 2889 | 2885 | $v$C3−H19(93) |
| 11 | 1660 | | 1660 | 1661 | $v$O4−C1(88) |
| 12 | 1607 | 1607 | 1605 | 1610 | $v$C2−C3(55), $\beta$H19−C3−C2(11) |
| 13 | 1596 | 1596 | 1596 | 1598 | $v$C7−C8(53), $v$O29−N28(23), $v$O30−N28(10) |
| 14 | 1584 | 1584 | 1582 | 1583 | $v$C9−C10(41), $v$C6−C7(11), $v$C8−C9(10) |
| 15 | 1534 | 1534 | 1535 | 1530 | $v$C12−C13(44), $v$O29−N28(23), $v$O30−N28(22), $v$C15−C16(21) |
| 16 | 1493 | | 1491 | 1490 | $v$C14−C15(39), $v$C11−C12(18), $v$C13−C14(18), $v$C11−C16(17) |
| 17 | | 1485 | 1484 | 1485 | $v$O29−N28(41), $v$O30−N28(20), $v$C7−C8(13), $v$C5−C6(11) |
| 18 | 1412 | 1412 | 1414 | 1416 | $\beta$H20−C6−C7(48), $\beta$H22−C9−C10(17), $\beta$H21−C7−C6(16), $\beta$H23−C9−C10(15) |
| 19 | | | 1405 | 1410 | $\beta$H25−C13−C12(39), $\beta$H26−C15−C16(16), $\beta$H27−C15−C16(14), $\beta$H24−C12−C13(13), |
| 20 | 1396 | 1396 | 1395 | 1399 | $v$C6−C7(48), $v$C9−C10(16), $\beta$H22−C9−C8(12) |
| 21 | 1348 | 1348 | 1348 | 1354 | $v$C12−C13(45), $v$C15−C16(24), $\beta$H26−C15−C16(12) |
| 22 | | 1325 | 1325 | 1331 | $v$O29−N28(40), $v$O30−N28(39), $\beta$O29−N28−O30(12) |
| 23 | 1317 | | 1317 | 1320 | $\beta$H19−C3−C2(44), $v$C5−C6(18), $v$C8−C9(16), $v$C6−C7(14), $v$C9−C10(14) |
| 24 | 1288 | | 1288 | 1285 | $\beta$H19−C3−C2(30), $v$C2−C3(10), $\beta$H20−C6−C7(10) |
| 25 | | 1293 | 1294 | 1290 | $v$C11−C12(40), $v$C14−C15(19), $v$C11−C16(18), $v$C13−C14(15) |
| 26 | 1215 | | 1216 | 1221 | $\beta$H25−C13−C12(39), $\beta$H24−C12−C13(19), $\beta$H27−C15−C16(18), $\beta$H26−C15−C16(16) |
| 27 | 1179 | 1182 | 1180 | 1183 | $\beta$H23−C9−C10(35), $\beta$H22−C9−C10(13), $\beta$H20−C6−C7(11), $\beta$H21−C7−C6(10), $\beta$H19−C3−C2(10), |
| 28 | | | 1163 | 1167 | $\beta$H18−C2−C1(43), $v$C1−C11(17) |
| 29 | | | 1159 | 1160 | $v$C1−C2(53), $v$C3−C5(17), $\beta$H18−C2−C1(13), $v$C1−C11(12) |
| 30 | 1148 | | 1150 | 1154 | $v$C3−C5(36), $v$C5−C6(14), $v$C9−C10(10), $\beta$H19−C3−C2(10) |
| 31 | 1132 | | 1133 | 1138 | $\beta$H20−C6−C7(47), $\beta$H23−C9−C10(20), $\beta$H21−C7−C6(10) |
| 32 | 1108 | 1108 | 1110 | 112 | $\beta$H27−C15−C16(30), $\beta$H24−C12−C13(19), $\beta$H26−C15−C16(18), $\beta$H25−C13−C12(15) |
| 33 | | | 1097 | 1096 | $\beta$H21−C7−C6(32), $\beta$H24−C12−C13(20), $v$C15−C16(17), $v$C6−C7(16), $\beta$H23−C9−C10(12) |
| 34 | | | 1083 | 1085 | $\beta$H22−C9−C10(30), $\beta$H26−C15−C16(16), $\beta$H27−C15−C16(12), $v$C12−C13(12), |
| 35 | 1070 | 1070 | 1068 | 1065 | $v$N28−C8(31), $v$C8−C9(19), $v$C7−C8(17), $\beta$H21−C7−C6(13), $\beta$H22−C9−C10(11) |

*Contd….*

Table 2 — Comparison of the experimental (FTIR and FT-Raman) wavenumbers (cm⁻¹) and theoretical wavenumbers (cm⁻¹) of (2E)-1-(4-bromophenyl)-3-(4-nitrophenyl) prop-2-en-1-one calculated by B3LYP/6- 31+G (d) and CAM- B3LYP/6- 31+G (d). (*contd*)

| S. No. | Experimental (cm⁻¹) | | Calculated frequencies( cm⁻¹) Scaled | | ᵃPED (%) among types of internal coordinates |
|---|---|---|---|---|---|
| | FTIR | FT-Raman | B3LYP/ 6-31+G(d) | CAM-B3LYP/ 6-31+G(d) | |
| 36 | 1027 | 1028 | 1025 | 1028 | νC1−C2(30), νC11−C12(13), νC14−C15(10) |
| 37 | 1007 | | 1010 | 1005 | νC13−C14(34), νC14−C15(19), νC12−C13(11) |
| 38 | | | 994 | 995 | βC6−C7−C8(32), βC7−C8− C9 (16), γ C2−C3−C5−H19 (10) |
| 39 | 984 | 984 | 985 | 982 | γ C2−C3−C5−H19 (55), τH18−C2−C3−C5(22) |
| 40 | | | 926 | 925 | βC12−C11− C16 (30),βC13−C14− C15 (29), νC11−C16(14), νC11−C12(12) |
| 41 | 905 | | 906 | 900 | γ C12−C11−C13−H24(59), τH25−C13−C12−C11(31) |
| 42 | 892 | 892 | 893 | 895 | τH22−C9−C10−H23(40), τH20−C6−C7−H21(29), γ C9−C8−C10−H22 (10) |
| 43 | 855 | 857 | 855 | 858 | τH26−C15−C16−C27(80) |
| 44 | | | 840 | 845 | τH20−C6−C7−H21(49), τH22−C9−C10−H23(39) |
| 45 | 834 | | 835 | 830 | τH18−C2−C3−C5(44), γ C2−C3−C5−H19 (14), γ C7−C6−C8−H21 (11), γ O4−C2−C11−C1(11), |
| 46 | | | 829 | 824 | βC7−C8− C9 (16), βO29−N28−O30(11),νC7−C8(10) |
| 47 | 821 | | 820 | 822 | τH25−C15−C16−C11(71), γ C7−C6−C8−H21 (14), γ C9−C8−C10−H22 (10) |
| 48 | | | 793 | 796 | τH26−C13−C12−C11(31), γ C12−C11−C13−H24(15) |
| 49 | 789 | | 790 | 792 | τH25−C13−C12−C11(34), γ C9−C8−C10−H22 (20), γ C12−C11−C13−H24(15) |
| 50 | | | 768 | 770 | γ C7−C6−C8−H21 (57), γ C9−C8−C10−H22 (39) |
| 51 | 753 | 754 | 752 | 754 | βO29−N28−O30(38), βC7−C8− C9 (13) |
| 52 | 705 | 705 | 706 | 708 | γ O30−C8−O29−N28(12), βC13−C14− C15 (10) |
| 53 | | | 695 | 698 | βC13−C14− C15 (44), γ O30−C8−O29−N28(10) |
| 54 | 690 | | 692 | 695 | γ O30−C8−O29−N28(49), τC11−C16−C15−C14(20), τC11−C12−C13−C14(18) |
| 55 | 661 | | 660 | 664 | γ O30−C8−O29−N28(57), τC5−C6−C7−C8(12), τC5−C10−C9−C8(10) |
| 56 | | | 645 | 640 | βC5−C6−C7(63),βO29−N28−O30(16) |
| 57 | | 637 | 638 | 635 | γ O4−C1−C11−C1(55), βC6−C7−C8(10) |
| 58 | | 627 | 627 | 629 | βC6−C7−C8(66), βC2−C1−O4(11) |
| 59 | | 590 | 592 | 593 | βC14−C15− C16 (67), βC8−C9−C10(39) |
| 60 | 570 | | 573 | 569 | βC2−C1−O4(57), βC6−C7−C8(11) |
| 61 | 542 | 541 | 540 | 542 | βC2−C1− C11 (44), βC2−C1−O4(16) |
| 62 | 519 | 516 | 520 | 515 | βC8−N28−O29(60), βC7−C8− C28(15) |
| 63 | 489 | | 487 | 485 | τC6−C7−C8−C9(56), τC3−C5−C6−C7(10) |
| 64 | 466 | | 465 | 463 | τC13−C14−C15−C16(50), τC11−C16−C15−C14(10) |
| 65 | | | 416 | 418 | νBr17−C14(52), νC1−C11(17), βC2−C1−O4(16), |
| 66 | | | 380 | 375 | τC11−C16−C15−C14(67), νN28−C8(16) |
| 67 | | | 352 | 354 | τC11−C12−C13−C14(39), τC11−C16−C15−C14(10) |
| 68 | | | 316 | 319 | τC5−C10−C9−C8(46), τC5−C6−C7−C8(36) |
| 69 | | | 280 | 281 | βC3−C5− C6 (42), τC6−C7−C8−C8(11) |
| 70 | | 266 | 265 | 266 | τC3−C5−C6−C7(48), τC6−C7−C8−N28(11), τC1−C2−C3−C5(10) |
| 71 | | 215 | 215 | 218 | βC15−C14− Br17(47), βC1−C11− C12(13) |
| 72 | | | 188 | 180 | τC1−C11−C16−C15(51), νBr17−C14(18), τC16−C15−C14−Br17(14) |

*Contd…*

Table 2 — Comparison of the experimental (FTIR and FT-Raman) wavenumbers (cm$^{-1}$) and theoretical wavenumbers (cm$^{-1}$) of (2E)-1-(4-bromophenyl)-3-(4-nitrophenyl) prop-2-en-1-one calculated by B3LYP/6- 31+G (d) and CAM- B3LYP/6- 31+G (d). (*contd*)

| S. No. | Experimental (cm$^{-1}$) | | Calculated Frequencies ( cm$^{-1}$) Scaled | | $^a$PED (%) among types of internal coordinates |
|---|---|---|---|---|---|
| | FTIR | FT-Raman | B3LYP/ 6-31+G(d) | CAM-B3LYP/ 6-31+G(d) | |
| 73 | | 176 | 175 | 176 | τC16−C15−C14−Br17(46), τC1−C11−C16−C15(14), βC7−C8− C28(14) |
| 74 | | 162 | 160 | 163 | βC7−C8− C28(57), τC3−C2−C1−C11(22) |
| 75 | | | 132 | 132 | τC6−C7−C8−N28(65), τC3−C2−C1−C11(22) |
| 76 | | 115 | 114 | 116 | βC1−C11− C12(49), βC15−C14− Br17(23), τC3−C2−C1−C11(10) |
| 77 | | | 95 | 93 | τC3−C2−C1−C11(39), βC1−C2−C3(11), βC2−C1− C11 (11), τC1−C2−C3−C5(10) |
| 78 | | 85 | 86 | 85 | τC3−C2−C1−C11(36), γC2−C1− O4(15) |
| 79 | | 70 | 73 | 75 | τC16−C15−C14−Br17(20), τC1−C11−C16−C15(17), βC3−C5− C6 (16), βC3−C5− C6 (14) |
| 80 | | 61 | 60 | 62 | τC2−C1−C11−C16(49), τC1−C11−C12−H24(17) |
| 81 | | | 35 | 38 | τC7−C8−N28−O29(92) |
| 82 | | | 25 | 26 | τC3−C5−C6−C7(26), τC1−C2−C3−C5(25), τC2−C1−C11−C16(21) |
| 83 | | | 21 | 22 | βC2−C1− C11 (20), βC1−C2−C3(18), τC1−C11−C16−C15(14) τC1−C2−C3−C5(11), βC3−C5− C6 (10), |
| 84 | | | 20 | 20 | τC2−C3−C5−C6(73), τC3−C2−C1−C11(10) |

ν; Stretching, β; in-plane bending, γ; out-of-plane bending, τ; torsion.
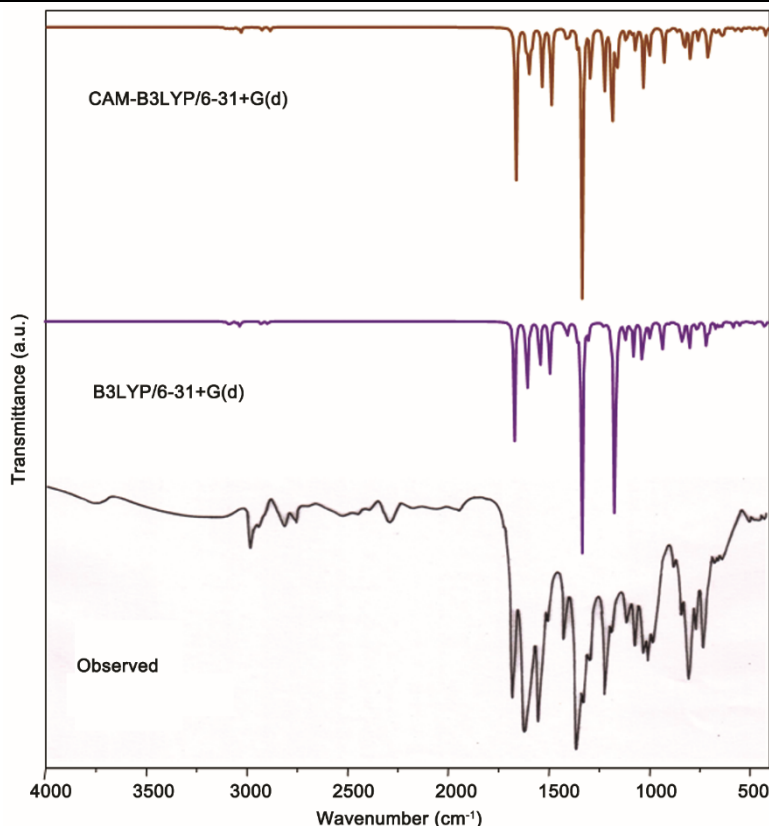$^a$ Potential energy distribution



Fig. 2 — Experimental and calculated FTIR spectra of (2E)-1-(4-bromophenyl)-3-(4-nitrophenyl) prop-2-en-1-one.
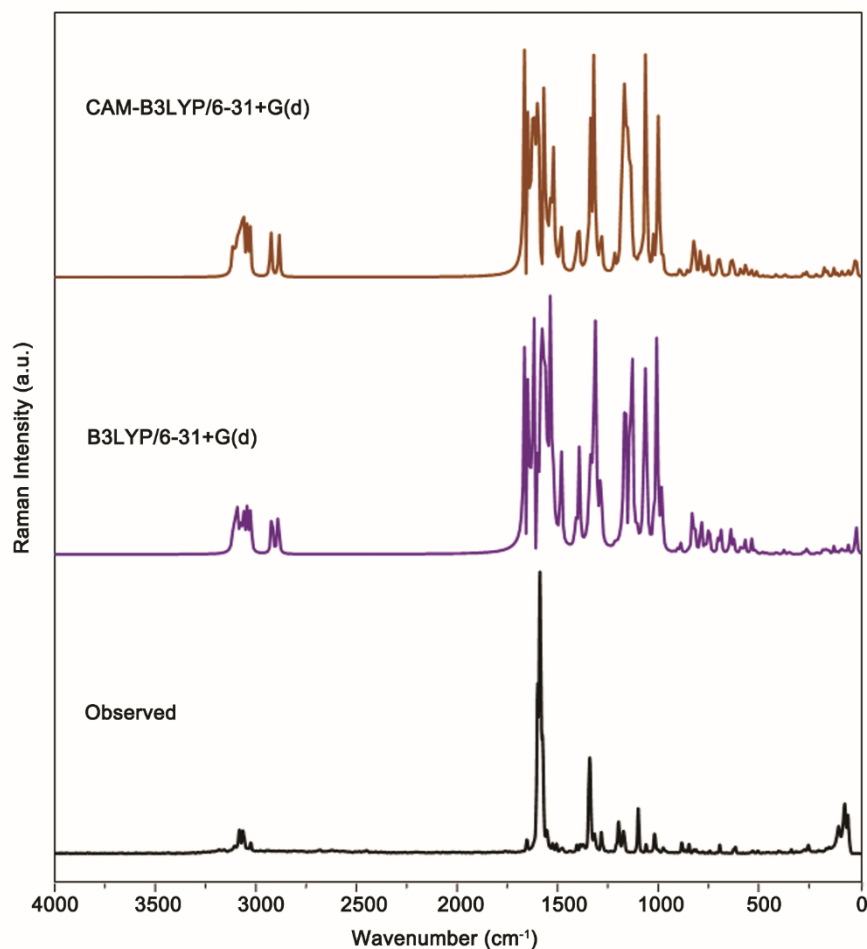
Fig. 3 — Experimental and calculated FT-Raman spectra of (2E)-1-(4-bromophenyl)-3-(4-nitrophenyl) prop-2-en-1-one.

The involvement of the $NO_2$ group in $\pi$-conjugation favours the intra-molecular charge transfer from the donor to the acceptor and gives rise to a large variation of the dipole moment, thus gaining a strong infrared and Raman activity.

The scissoring, wagging, rocking and twisting modes of $NO_2$ group are identified in their characteristic regions and contribute to several normal modes. The $NO_2$ scissoring vibration occurs in the range 880–710 $cm^{-1}$. In the present work, vibrations at 753 $cm^{-1}$ in the FTIR and 754 $cm^{-1}$ in the FT-Raman spectrum are assigned to $NO_2$ scissoring mode. The theoretically computed values at 753 and 754 $cm^{-1}$ are well supported by FTIR and in FT-Raman spectra. In aromatic compounds, the wagging mode of $NO_2$ is assigned at 780 $\pm$ 50 $cm^{-1}$ with a moderate to strong intensity. For the present molecule wagging vibrations of $NO_2$ group computed at 706, 692 and 664 $cm^{-1}$ by B3LYP/6-31+G(d) method coincide well with bands at 705, 690 and 661 $cm^{-1}$ in the FTIR spectrum and weak bands at 705 $cm^{-1}$ in the FT-Raman spectrum. The rocking mode of $NO_2$ is active in the region 540 $\pm$ 45 $cm^{-1}$ in aromatic compounds. In the present case, the rocking modes of $NO_2$ group at 520 and 515 $cm^{-1}$ in B3LYP and CAM-B3LYP method are supported by experimental observation at 519 $cm^{-1}$ in the FTIR spectrum and 516 $cm^{-1}$ in the FT-Raman spectrum. The frequency computed theoretically by B3LYP/6-31+G (d) method at 35 $cm^{-1}$ is assigned to torsion mode of $NO_2$ group. As the torsion vibration is very anharmonic, its frequency is difficult to reproduce within the harmonic approach.

The C=O stretching vibration band can be easily identified from the FTIR and FT-Raman spectra, because of the degree of conjugation, strength and polarizations. The characteristic infrared absorption frequencies of carbonyl group have been extensively investigated. The C=O stretching vibration band can be

easily identified in the FTIR and FT-Raman spectrum as due to high degree of conjugation, the strength and polarization are increased. The carbon–oxygen double bond is formed by π–π bonding between carbon and oxygen. Because of the different electronegativities of carbon and oxygen atoms, the bonding electrons are not equally distributed between the two atoms. The carbonyl stretching vibrations in ketones are expected in the region[17,18] 1715– 1680 cm$^{-1}$. In our case, the C=O stretching band is observed at 1660 cm$^{-1}$ in FTIR spectrum. The remainder of the observed and calculated wavenumbers and their assignments of the compound are shown in Table 2.

The vibrations of the ethylenic bridge are highly sensitive to the degree of charge transfer between the donor and the acceptor groups, hence such stretching modes are of particular interest for spectroscopists[17,19]. The sharp intense band observed at 1607 cm$^{-1}$ in both FTIR and FT-Raman spectrum is assigned to C2=C3 stretching mode. The aliphatic C−H stretching bands are expected between 3050 and 3000 cm$^{-1}$. The C−H stretching modes are predicted experimentally at 2923 and 2887 cm$^{-1}$ in FTIR and FT-Raman spectrum, respectively. The bands corresponding to in-plane and out-of-plane deformations are observed as expected, in the regions 1500–1000 cm$^{-1}$ and 1000– 750 cm$^{-1}$, respectively.

The identification of C−N vibrations is a difficult task, because of the mixing of vibration in this region. However with the help of force field calculations, the C−N vibrations are identified and assigned in this study. The very weak band observed at 1070 cm$^{-1}$ in both FTIR and FT- Raman spectrum is attributed to the C–N stretching mode. The corresponding IR band is identified at the same wavenumber. The in-plane bending and out-of-plane bending vibrations of C−N are given in Table 2.

Bromine compounds absorb strongly in the range of 650 –485 cm$^{-1}$ due to C–Br stretching vibrations[20]. C–Br stretching vibrations are not observed experimentally. With the help PED contributions, calculated wavenumber for C–Br stretching is shown in Table 2. FT-Raman band at 215 cm$^{-1}$ are assigned to the C–Br in-plane bending vibrations. The C–Br out-of-plane bending vibration is obtained at 176 cm$^{-1}$ in FT-Raman and theoretically agrees with the medium contribution of PED.

### 5.3 Molecular properties

In simple molecular orbital theory approaches, the global chemical reactivity descriptors of molecules such as hardness, chemical potential, softness, electronegativity and electrophilicity index as well as local reactivity have been defined[21,22]. The smaller ionization potential (higher $E_{HOMO}$) and higher electron affinity (lower $E_{LUMO}$) correspond to stronger CT interaction. This statement accounts for smaller η. The $E_{HOMO}$, $E_{LUMO}$, χ, η values and electronic properties of for the molecular system have been compared with chalcone derivative[23] and are given in Table 3. The electron density-based local reactivity descriptors such as Fukui functions were proposed to explain the chemical selectivity or reactivity at a particular site of a chemical system[24]. Electron density is a property that contains all the information about the molecular system and plays an important role in calculating the chemical quantities. Yang and Mortier[25] proposed a finite difference approach to calculate Fukui function indices, i.e., nucleophilic, electrophilic and radical attacks. In the present study, the optimized molecular geometry was utilized in single-point energy calculations, which have been performed at the DFT for the anions and cations of the molecule using the ground state with doublet multiplicity. The individual atomic charges calculated by natural population analysis (NPA) have been used to calculate the Fukui function. Using NPA atomic charges of neutral, cation and anion state of BP4NP, Fukui functions ($f_k^+, f_k^-, f_k^0$), local softness ($s_k^+, s_k^-, s_k^0$) and local electrophilicity indices ($\omega_k^+, \omega_k^-, \omega_k^0$) are calculated[24,25] by B3LYP/6-31+G (d). The superscripts +, −, 0 signs show nucleophilic, electrophilic and radical attack, respectively. Fukui functions, local softness and local electrophilicity indices for selected atomic sites of title compound have been listed in Table 4. The maximum values of all the three $f_k^-, s_k^-, \omega_k^-$ local reactive descriptors at carbonyl group ($C_1=O_4$) atom C1 and

Table 3 — Comparison of reactive descriptors calculations of (2E)-1-(4-bromophenyl)-3-(4-nitrophenyl) prop-2-en-1-one.

| Parameters | BP4NP | [a]BP2CP |
|---|---|---|
| Ionisation potential ($E_{HOMO}$) | -6.960 | -6.669 |
| Electron affinity ($E_{LUMO}$) | -3.048 | -2.198 |
| Optical gap $(\Delta E)$ | 3.911 | 4.4706 |
| Hardness(η) | -1.955 | -2.235 |
| Electronegativity(χ) | -5.004 | -4.434 |
| Chemical potential(φ) | 5.004 | 4.434 |
| Global Electrophilicity(ω) | -6.402 | -4.398 |

[a]Ref.[23]

NO$_2$ group atom N$_{28}$ indicate that this site is prone to electrophilic attack.

The frontier molecular orbital and electrostatic potential plot for BP4NP using B3LYP/6-31+G (d) level are displayed in Figs 4 and 5. A portion of a molecule that has a negative electrostatic potential will be susceptible to electrophilic attack—the more negative the better. It is not as straightforward to use electrostatic potentials to predict nucleophilic attack[21]. To predict reactive sites of electrophilic and nucleophilic attacks for the investigated molecule, MEP at the B3LYP level optimized geometry was calculated using GAUSSVIEW[10] program. The different values of the electrostatic potential at the MEP surface are represented by different colors; red, blue and green representing the regions of most negative, most positive and zero electrostatic potential, respectively. The negative electrostatic potential corresponds to an attraction of the proton by the aggregate electron density in the molecule (shades of red), while the positive electrostatic potential corresponds to the repulsion of the proton by the atomic nuclei (shade of blue) shown in Fig. 5. From the MEP it is evident that the negative region covers the C=O and NO$_2$ group and the positive region is over the phenyl rings. Also, the variation of $\chi$ values is supported by the electrostatic potential. Large $\chi$ values characterize acids and small $\chi$ values are found for bases, electron will be partially transferred from the one of low $\chi$ to that of high $\chi$ (electrons flow from high chemical potential to low chemical potential). Negative $\chi$ is equal to the electronic chemical potential[22] ($\varphi = -\chi$).

**5.4 Natural bonding orbital analysis**

Various second-order interactions between the filled orbitals of one subsystem and vacant orbitals of another subsystem are the measure of the delocalization or hyperconjugation interactions. The hyper conjugation interaction energy was deduced from the second-order perturbation approach[26]:

$$E(2) = \Delta E_{ij} = q_i \frac{F(i,j)^2}{\varepsilon_j - \varepsilon_i}$$

where $E(2)$ is stabilization energy, $q_i$ is the donor orbital occupancy, $\varepsilon_i$ and $\varepsilon_j$ are diagonal elements and $F(i, j)$ is the off-diagonal NBO Fock matrix element between the donor ($i$) and acceptor ($j$) NBO orbitals. The hyperconjugative interaction energy was deduced from the second-order perturbation approach. Delocalization of electron density between occupied Lewis-type (bond or lone pair) NBO orbitals and formally unoccupied (antibond or Rydberg) non-Lewis NBO orbitals corresponds to a stabilizing donor–acceptor interaction. The corresponding results have been given as shown in Table 5. In NBO analysis, large $E(2)$ value shows the intensive interaction between electron-donors and electron-acceptors and the greater the extent of conjugation of the whole system, the possible intensive interaction is given in Table 5. The

Table 4 — Fukui functions ( $f_k^+$, $f_k^-$, $f_k^0$ ), local softness ( $S_k^+$, $S_k^-$, $S_k^0$ ) and local electrophilicity indices (calculated by B3LYP/6-31+G (d) for the title molecule.

| Atoms | Fukui functions | | | Local softness | | | Local electrophilicity indices | | |
|---|---|---|---|---|---|---|---|---|---|
| | $f_k^+$ | $f_k^-$ | $f_k^0$ | $s_k^+$ | $s_k^-$ | $s_k^0$ | $\omega_k^+$ | $\omega_k^-$ | $\omega_k^0$ |
| C1 | -0.0728 | 0.0041 | -0.0344 | -0.0281 | 0.0016 | -0.0132 | -0.2382 | 0.0135 | -0.1124 |
| C2 | -0.0635 | -0.0311 | -0.0473 | -0.0244 | -0.0120 | -0.0182 | -0.2075 | -0.1017 | -0.1546 |
| C3 | -0.0519 | -0.0572 | -0.0545 | -0.0200 | -0.0220 | -0.0210 | -0.1696 | -0.1870 | -0.1783 |
| O4 | -0.0910 | -0.1826 | -0.1368 | -0.0350 | -0.0703 | -0.0527 | -0.2975 | -0.5971 | -0.4473 |
| C10 | -0.0338 | -0.0329 | -0.0334 | -0.0130 | -0.0127 | -0.0128 | -0.1105 | -0.1076 | -0.1091 |
| C11 | 0.0305 | -0.0485 | -0.0090 | 0.0117 | -0.0187 | -0.0035 | 0.0996 | -0.1584 | -0.0294 |
| C14 | -0.0265 | -0.0283 | -0.0274 | -0.0102 | -0.0109 | -0.0106 | -0.0866 | -0.0927 | -0.0896 |
| Br17 | -0.0563 | -0.1780 | -0.1172 | -0.0217 | -0.0686 | -0.0451 | -0.1841 | -0.5821 | -0.3831 |
| H20 | -0.0246 | -0.0127 | -0.0186 | -0.0095 | -0.0049 | -0.0072 | -0.0803 | -0.0415 | -0.0609 |
| H27 | 0.0020 | -0.0148 | -0.0064 | 0.0008 | -0.0057 | -0.0025 | 0.0064 | -0.0485 | -0.0210 |
| N28 | -0.0338 | 0.0124 | -0.0107 | -0.0130 | 0.0048 | -0.0041 | -0.1105 | 0.0406 | -0.0349 |
| O29 | -0.1011 | -0.0377 | -0.0694 | -0.0389 | -0.0145 | -0.0267 | -0.3305 | -0.1231 | -0.2268 |
| O30 | -0.1007 | -0.0375 | -0.0691 | -0.0388 | -0.0144 | -0.0266 | -0.3294 | -0.1226 | -0.2260 |
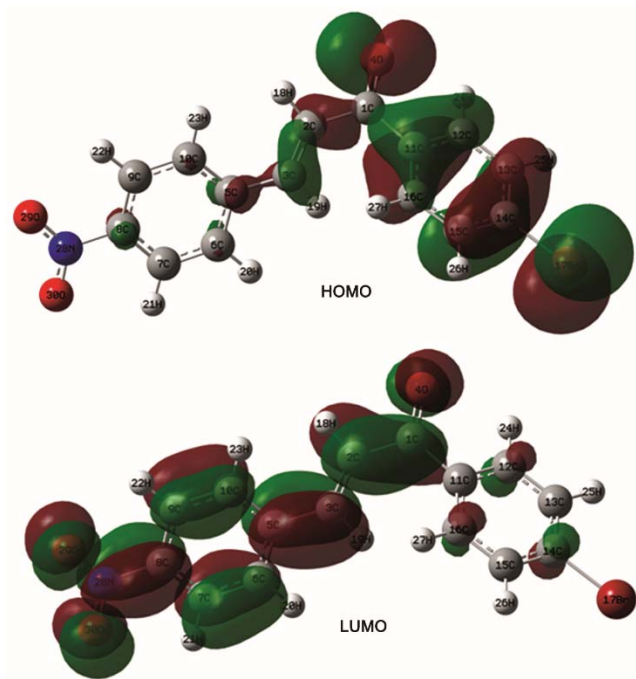
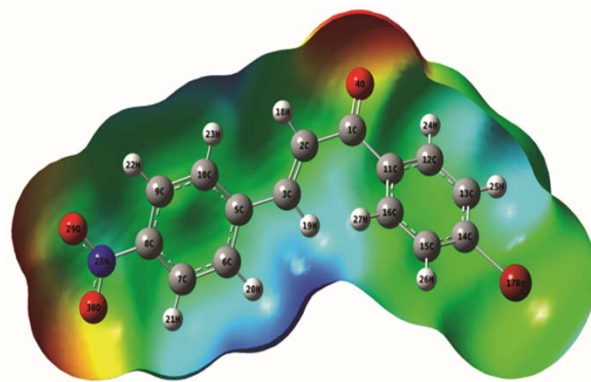Fig. 4 — HOMO and LUMO plot of (2E)-1-(4-bromophenyl)-3-(4-nitrophenyl) prop-2-en-1-one.



Fig. 5 — Molecular electrostatic potential surface of (2E)-1-(4-bromophenyl)-3-(4-nitrophenyl) prop-2-en-1-one.

second-order perturbation theory analysis of Fock matrix in NBO basis shows strong intra molecular hyperconjugative interactions of π electrons. The intra-molecular rehybridization and delocalization of energy density within the molecule result in ICT, causing stabilization of the system. The C–Br and C–O stretching modes can be used as a good probe for evaluating the bonding configuration around the bromine and oxygen atom and the electronic distribution of the benzene molecule. The π*(C14 - C15) of the NBO conjugator with π*(C11 - C16) resulting in an enormous stabilization of 222.4 kcal/mol as shown in the Table 5. This is the highest energy from all interaction. The π*(C14 - C15) of the

NBO orbital further conjugate with π*(C12 - C13) resulting in a stabilization of 124.52 kcal/mol as shown in Table 5. Also an important hyperconjugative interaction is observed between lone pair LP (3) O30 and π*(N28 - O29) which is about 164.23 kcal/mol.

**5.5 Electronic absorption spectrum**

In order to obtain a more intuitive description of the band assignments of the electronic absorption spectra and the trends in the NLO behaviours of the studied compound, TD-DFT method at the CAM-B3LYP/6-31+G (d) level in the gas phase and different solvent phase has been performed. In addition to the gas phase the IEFPCM has been used to examine the solvent

effect on the electronic spectral properties. IEFPCM has shown to be very effective tool, since it can provide conceptually simple, but accurate and physically well-founded, description of solvent effects on several molecular properties. It offers a unified and well sound framework for the evaluation of all the interaction contributions both for isotropic and anisotropic solution.

The calculated wavelengths ($\lambda$, nm), excited state transition energies ($\Delta E_{gm}$, eV), oscillator strengths ($f_{os}$), and major molecular orbital transitions of compound calculated using TD-CAM-B3LYP functionals with 6−31+G(d) associated with IEFPCM in polar protic and polar aprotic solvents has been summarized in Table 6. The major contributions of the HOMO-LUMO transitions are designated with the aid of Gausssum 2.2 program[27]. The absorption spectra for compound have been plotted in Fig. 6. The first excited states of compound have generated by one-electron transfer from HOMO to LUMO. HOMO and LUMO are related to some chemical

properties of complexes such as redox and electronic transition, etc. The HOMOs and LUMOs have been plotted in Fig. 4. The conjugated molecules are characterized by a small HOMO–LUMO energy separation which is the electronic absorption corresponding to the intra-molecular charge transition from the ground to the first excited state and is mainly described by one electron excitation from the end capping electron donor groups (HOMO) to the efficient acceptor groups (LUMO) through $\pi$ conjugated path. The charge transfer interaction between HOMO and LUMO orbital of a structure, transition state transition of $\pi$–$\pi^*$ type is observed with regard to the molecular orbital theory. In BP4NP, LUMO the substitution electron acceptor group of $NO_2$ atom is placed on the benzoyl moiety which is $\pi$ nature and the HOMO is located over the electron donor group of Br atom on the phenylene group consequently the HOMO $\rightarrow$ LUMO transition implies an electron density transfer to $NO_2$ substituted benzene ring from Br atom.

Table 5 — Selected second order perturbation energies of the (2E)-1-(4-bromophenyl)-3-(4-nitrophenyl) prop-2-en-1-one calculated using B3LYP/ 6-31+G (d) chemistry level.

| Donor | ED($i$)e | Acceptor ($j$) | ED($j$)e | E(2) (kcal/mol) | E($i$)-E($j$) (a. u.) | F($i$,$j$) (a. u.) |
|---|---|---|---|---|---|---|
| $\pi$(C5 - C6) | 1.6022 | $\pi^*$(C7 - C8) | 0.37403 | 23.26 | 0.27 | 0.072 |
| $\pi$(C7 - C8) | 1.6387 | $\pi^*$( C5 - C6) | 0.36363 | 18.22 | 0.29 | 0.065 |
| $\pi$(C7 - C 8) | 1.6387 | $\pi^*$(C9 - C10) | 0.26964 | 19.72 | 0.3 | 0.07 |
| $\pi$(C 7 - C8) | 1.6387 | $\pi^*$(N28 - O29) | 0.62801 | 27.36 | 0.15 | 0.062 |
| $\pi$(C9 - C10) | 1.6622 | $\pi^*$(C5 - C6) | 0.36363 | 20.55 | 0.28 | 0.069 |
| $\pi$(C9 - C10) | 1.6621 | $\pi^*$(C7 - C8) | 0.37403 | 19.66 | 0.28 | 0.067 |
| $\pi$(C11 - C16) | 1.6412 | $\pi^*$(C12 - C13) | 0.2825 | 19.80 | 0.29 | 0.069 |
| $\pi$(C11 - C16) | 1.6412 | $\pi^*$(C14 - C15) | 0.3781 | 20.76 | 0.27 | 0.067 |
| $\pi$(C12 - C13) | 1.6547 | $\pi^*$(C11 - C16) | 0.3683 | 18.81 | 0.28 | 0.065 |
| $\pi$(C12 - C13) | 1.6547 | $\pi^*$(C14 - C15) | 0.3781 | 22.08 | 0.27 | 0.069 |
| $\pi$(C14 - C15) | 1.6691 | $\pi^*$( C11 - C16) | 0.3683 | 19.58 | 0.3 | 0.069 |
| $\pi$(C14 - C15) | 1.6691 | $\pi^*$( C12 - C13) | 0.2825 | 17.33 | 0.3 | 0.065 |
| LP (2) O4 | 1.8883 | $\sigma^*$ (C1 - C2) | 0.0545 | 18.79 | 0.7 | 0.104 |
| LP (2) O 4 | 1.8883 | $\sigma^*$ (C1 - C11) | 0.0670 | 19.47 | 0.69 | 0.104 |
| LP (2) O29 | 1.8978 | $\sigma^*$ (N28 - O30) | 0.0567 | 19.24 | 0.71 | 0.105 |
| LP (2) O30 | 1.8977 | $\sigma^*$ (N28 - O29) | 0.6280 | 19.23 | 0.71 | 0.105 |
| LP (3) O30 | 1.4431 | $\pi^*$(N28 - O29) | 0.6280 | 164.23 | 0.14 | 0.139 |
| $\pi^*$(C1 - O4) | 0.1742 | $\pi^*$(C2 - C3) | 0.0960 | 41.06 | 0.02 | 0.066 |
| $\pi^*$(C5 - C6) | 0.3636 | $\pi^*$(C2 - C3) | 0.0960 | 60.26 | 0.02 | 0.064 |
| $\pi^*$(C14 - C15) | 0.3781 | $\pi^*$(C11 - C16) | 0.3683 | 222.43 | 0.01 | 0.084 |
| $\pi^*$(C14 - C15) | 0.3781 | $\pi^*$(C12 - C13) | 0.2825 | 124.52 | 0.02 | 0.078 |

ED: Electron density

[a]E(2) means energy of hyper conjugative interaction (stabilization energy).

[b]Energy difference between donor and acceptor $i$ and $j$ NBO orbitals.

[c]F($i$, $j$) is the Fock matrix element between $i$ and $j$ NBO orbitals

Table 6 — Wavelengths (λ), excited state transition energies (E), oscillator strengths ($f_{os}$), and major molecular orbital contributions of (2E)-1-(4-bromophenyl)-3-(4-nitroophenyl) prop-2-en-1-one calculated using TD-DFT method at the CAM-B3LYP/6-31+G (d) level in gas phase and different solvent phase.

|  | Energy (eV) | λ (nm) | Oscillator strength ($f_{os}$) | Major contributions |
|---|---|---|---|---|
| Gas phase | 4.3439 | 285 | 0.9424 | HOMO-1->LUMO (88%) |
| Tetrahydrafuran (THF) | 4.1494 | 298 | 1.0351 | HOMO-1->LUMO (48%), HOMO->LUMO (41%) |
| Methanol | 4.1431 | 299 | 1.0173 | HOMO->LUMO (82%) |
| Water | 4.1385 | 300 | 1.0171 | HOMO->LUMO (84%) |
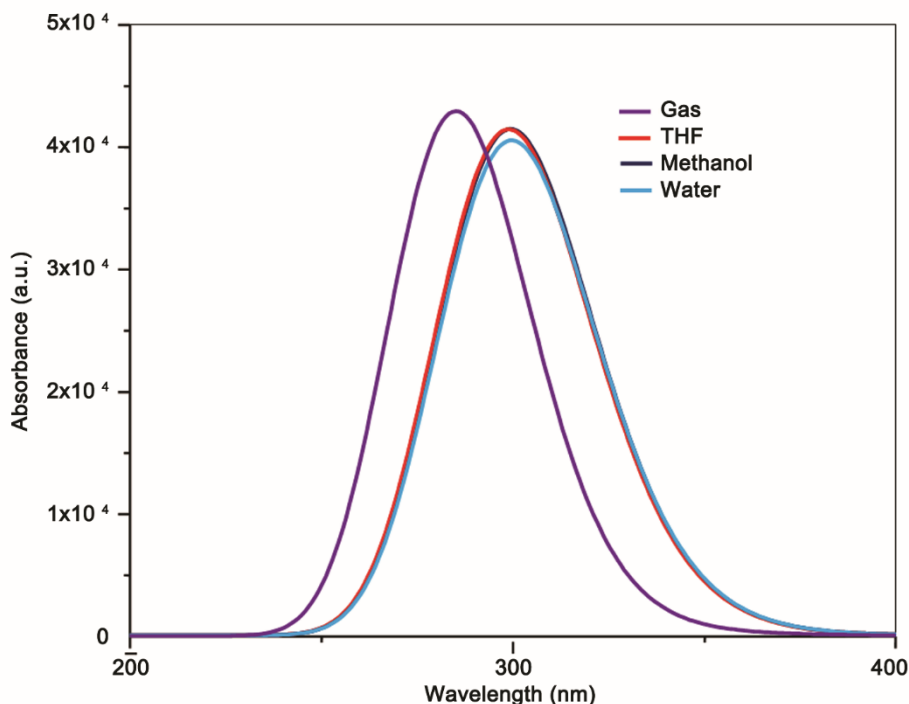


Fig. 6 — UV-Vis spectra of (2E)-1-(4-bromophenyl)-3-(4-nitrophenyl) prop-2-en-1-one.

**5.6 Static and dynamic NLO property**

Calculation of microscopic NLO property with long-range corrections ("LC" and "ω" methods) performs roughly equally among them, but improves the accuracy significantly over standard hybrids[28]. LC-DFT method with CAM-B3LYP functional is a procedure used here to find out approximate values and can be a means of understanding both static and dynamic hyperpolarizabilities of BP4NP. In this study, in addition to the static linear polarizabilities α(0;0), first order β(0;0,0) and second order γ(0; 0, 0, 0), hyperpolarizabilities, the processes for dynamic (hyper) polarizabilities have also been considered: frequency-dependent linear polarizabilities α(-ω; ω), second harmonic generation (SHG) β(-2ω; ω, ω, ω), third harmonic generation (THG) γ(-3ω; ω, ω, ω). Some significant calculated magnitudes of the static

and frequency dependent linear polarizabilities first- and second- order hyperpolarizabilities are shown in Tables 7 and 8, respectively. Virtually high-order NLO effects in organic molecules originate from a strong intra-molecular donor -acceptor interaction. Due to the ability of electron donor to donate electrons is enhanced, resulting in the decrease of frontier molecular orbitals energy gap and thus the increase of α(0; 0), first β(0;0,0) and second γ(0; 0, 0, 0).

We calculated the frequency-dependent first and second hyperpolarizability of the studied system by using CAM-B3LYP/ 6-31G+G(d) method. Generally, the molecular hyperpolarizabilities β(−2ω; ω, ω) have been measured in a fundamental incident wavelength which has a second harmonic far enough from the absorption bands to avoid the over measure of β values due to resonance effects[29,30]. Hence, two near resonant

wavelength of ω=0.0428 a.u. (1064 nm) and ω=0.0340 a.u. (1340 nm), one non-resonant wavelength of ω=0.0239 a.u. (1907 nm) are adopted to compute the frequency dependence. As shown in Table 8, the magnitude of the frequency-dependent first- and second-order hyperpolarizability increases with the increasing frequency (that is, the decrease of the wavelength λ of incident light)[29]. The values of β(−2ω;ω,ω) in the BP4NP are larger than that of β(−ω;ω,0), and both of the β(−2ω;ω,ω) and β(−ω;ω,0) values are larger than the corresponding static β values. Thus, β (−2ω; ω,ω) exhibits the largest frequency dispersion. The γ values depend on a number of factors, which include extent of π-electron conjugation, the dimensionality of the molecules and the nature of substituent. The role of phenyl rings in determining the NLO response in π conjugate chalcone derivatives, since it can act either as the donor or the bridging moiety of the donor- (π conjugate-bridge)-acceptor system. However, in presence of strong donor–acceptor substituent, the phenyl rings mostly acts as a bridge and are mainly responsible for the dispersion- free and frequency-dependent second hyperpolarizabilities with

non-zero values as microscopic NLO response of the investigated molecule.

### 5.7 Solvent effects on NLO property

In this investigation, the solvent effects on α, β and γ of BP4NP is observed in solvents of different polarity tetrahydrofuran (THF), acetone (polar aprotic solvent), ethanol (polar solvent), water (protic solvent) using IEFPCM model with CPDFT method by CAM-B3LYP/6-31+G(d) for frequency dependent case at 1064 nm (ω=0.0428 a.u). The effect of the solvent changes on linear polarizabilities, first order hyperpolarizabilities (SHG) and second order hyperpolarizabilities (THG) tensor are shown in Table 9. The electronic effect due to the solvent results in large increases of both the linear and nonlinear responses. We have demonstrated that the electronic effect due to the solvent results in large increases of both the linear and nonlinear responses. The most important feature of these calculations performed here is useful in providing a detailed interpretation of the molecular polarizabilities and in understanding their solvent dependence. They can be directly exploited to optimize organic materials for NLO applications.

### 5.8 Vibrational contributions on NLO property

Vibrational corrections originating from the coupling between the electronic and the nuclear motions are sometimes important in obtaining predictive accuracy for molecular (hyper) polarizabilities. Indeed, the application of an external electric field to a system can induce some distortions

Table 7 — The static linear polarizability (α), static anisotropic polarizability (Δα), dipole moment (μ), static first-order hyperpolarizability (β) and static second-order hyperpolarizability (γ) values of (2E)-1-(4-bromophenyl)-3-(2-nitrophenyl) prop-2-en-1-one in gas phase.

| Parameters | CAM-3LYP/ 6-31G+(d) |
|---|---|
| α×10^{-23} (esu) | 3.0021 |
| Δα×10^{-23} (esu) | 2.9121 |
| μ (Debye) | 2.6755 |
| β×10^{-30} esu | 9.7063 |
| γ×10^{-35} esu | 5.7889 |

Table 8 — The dynamic linear polarizability (α ×10^{−23} esu), dynamic anisotropic polarizability (Δα ×10^{−23} esu), dynamic first-order hyperpolarizability (β × 10^{-30} esu) and dynamic second-order hyperpolarizability (γ× 10^{-35} esu) values of (2E)-1-(4-bromophenyl)-3-(4-nitrophenyl) prop-2-en-1-one in gas phase.

| Parameters | ω=0.0239 a.u. (1907 nm) | ω=0.0340 a.u. (1340 nm) | ω=0.0428 a.u. (1064 nm) |
|---|---|---|---|
| α (-ω, ω) | 3.0235 | 3.0463 | 3.0736 |
| Δα (-ω, ω) | 2.9514 | 2.9934 | 3.0443 |
| β(-ω,ω,0) | 10.1285 | 7.4978 | 11.2841 |
| β(-2ω,ω,ω) | 11.1686 | 13.1009 | 16.0339 |
| γ(-ω,ω,0) | 5.1647 | 5.4404 | 5.7889 |
| γ(-3ω,ω,ω) | 5.7259 | 6.7916 | 8.4627 |

Table 9 — The static and dynamic linear polarizability (α ×10^{−23} esu), anisotropic polarizability (Δα ×10^{−23} esu), first-order hyperpolarizability (β × 10^{-30} esu) and second-order hyperpolarizability (γ× 10^{-35} esu) values of (2E)-1-(4-bromophenyl)-3-(4-nitrophenyl)prop-2-en-1-one in different solvent phase with IEFPCM model have been evaluated by couple perturbed (CP)DFT method, CAM-B3LYP functional at ω=0.0428 a.u.

| Parameter | Polar protic solvent | | Polar aprotic solvent | |
|---|---|---|---|---|
| | Water | Ethanol | THF | Acetone |
| α (0,0) | 3.9430 | 3.8942 | 3.7450 | 3.8796 |
| Δα (0,0) | 3.6056 | 3.5809 | 3.5000 | 3.5732 |
| α (-ω, ω) | 3.3956 | 3.4131 | 3.4369 | 3.5001 |
| Δα (-ω, ω) | 3.3958 | 3.4067 | 3.4149 | 3.1824 |
| β (0,0,0) | 21.8260 | 20.9673 | 18.9688 | 20.7706 |
| β(-ω,ω,0) | 19.3022 | 19.2199 | 18.6254 | 19.1202 |
| β(-2ω,ω,ω) | 25.3989 | 25.5610 | 25.4098 | 25.4611 |
| γ (0,0,0) | 12.9830 | 12.4953 | 11.0407 | 19.1202 |
| γ(-ω,ω,0) | 12.0698 | 11.9028 | 11.1937 | 11.8088 |
| γ(-3ω,ω,ω) | 5.0232 | 15.9327 | 4.8760 | 4.9900 |

of the nuclear, in addition to the electronic motions which lead to vibrational contributions to the (hyper) polarizabilities[31,32]. The intra-molecular charge transfer from donor to accepter group through a single–double bond conjugated path can induce large variations of both the molecular dipole moment and the molecular polarizability, making IR and Raman activity strong at the same time. The experimental spectroscopic behaviour described above is well accounted by ab initio calculations in π- conjugated systems that predict exceptionally large Raman cross sections and infrared intensities for the same normal modes[33]. The potential application of BP4NP in the field of nonlinear optics demands the investigation of the contribution of FTIR and FT-Raman active vibrational modes to the hyperpolarizability enhancement. Selection rule predicts that the ring C–C stretching bands at 1607, 1596, 1584, 1534, 1396, 1348, 1027 cm$^{-1}$ observed in FTIR have their counterparts in FT-Raman at 1607, 1596, 1584, 1534, 1396, 1348, 1028 cm$^{-1}$, respectively, and their relative intensities are comparable. In the case of chalcone, we expect that the stretching of the C=O bond is the most relevant motion for the vibrational averaging of the non-linear properties. The vibrational averaging has a little effect on the calculated polarizability, and a greater influence on the longitudinal component of the hyperpolarizability. It is worth noting that in aqueous solution the vibrational correction to the β value is markedly greater than in gas phase. Thus it is advisable to consider both the solvent and the vibrational effects, and their possible coupling, to get reliable values of molecular nonlinear properties.

## 6 Conclusions

The complete molecular structural parameters, spectroscopic and NBO analysis of the compound are obtained with DFT/B3LYP and LC-DFT/CAM-B3LYP method using 6-31+G (d) basis set. The calculated harmonic vibrational frequencies with DFT/B3LYP and LC-DFT/CAM-B3LYP method using 6-31+G (d) basis set for the synthesized compound are consistent with the experimental spectra. The NBO analysis confirmed the hyperconjugative interaction formed by overlap of bonding and anti-bonding orbitals. The reactive descriptors and non-linear optical properties were found to be associated with a decreased HOMO-LUMO gap, which is a consequence of the enhanced charge transfer between the donor and the acceptor group, is responsible for hyperpolarizability *(β)*

enhancement, leading to non-linear activity of the title compound. The first order β (SHG) and second order γ (THG) hyperpolarizabilities obtained using the CAM-B3LYP method for the title compound demonstrate promising practical applications in nonlinear optics. The variation of β and γ values increase with raising the frequency of the incident light and the increasing degree of β(-2ω,ω,ω) and γ (-3ω,ω,ω) is larger than that of the β(-ω,ω,0) and γ(-ω,ω,0) respectively. The solvent effects on α, β and γ of the BP4NP have shown that electronic effects of the solvent result in large increase of both the linear (α) and non-linear responses (β and γ) whereas their effect on the geometry is negligible. BP4NP shows the noticeable second – and third– order nonlinearity and chalcone can be used as an effective π-bridge in the design of new organic NLO materials.

## Acknowledgment

## References
1  Garito F, Wong K Y & Zamani-Khamiri O, *Nonlinear optical and electroactive polymers*, Edited by Ulrich D & Prasad P, (Plenum: New York), 1987.
2  Işik D, Santato C, Barik S & Skene W G, *Organic Electronics*, 13 (2012) 3022.
3   Mishra A & Bäuerle P, *Angew Chem Int*, 51 (2012) 2020.
4  Yang Y, Xiao H, Wang H, Liu F, Bo S, Liu J, Qiu L, Zhen Z & Liu X, *J Mater Chem C*, 3 (2015) 11423.
5  Sarojini B K, Narayana B, Ashalatha B V, Indira J & Lobo K G, *J Cryst Growth*, 295 (2006) 54.
6  Poornesh P, Shettigar S, Umesh G, Manjunatha K B, Prakash K K, Sarojini B K & Narayana B, *Opt Mater*, 31 (2009) 854.
7  Sreevidya T V, Narayana B & Yathirajan H S, *Cent Eur J Chem*, 8 (2010) 174.
8  Harrison W T A, Yathirajan H S, Narayana B, Sreevidya T V & Sunil K, *Acta Cryst*, E62 (2006) 4829.
9  Frisch M J, Trucks G W & Schlegel H B, *Gaussian*, (Inc, Wallingford CT), 2009.
10 Dennington R, Keith T & Millam J, *Gauss View, Version 5, Semichem Inc*, Shawnee Mission, KS, 2009.
11 Jamroz M H, *Vibrational energy distribution analysis,* VEDA 4 Computer Program, Poland, 2004.
12 Glendening E D, Reed A E, Carpenter J E & Weinhold F, *NBO Version 3.1*, TCI, (University of Wisconsin: Madison),1998.
13 Keresztury G, Chalmers J M & Griffith P R, *Raman spectroscopy: Theory in handbook of vibrational spectroscopy,* 1 (John Wiley & Sons Ltd: New York), 2002.
14 Champagne B, Botek E, Nakano M,  Nitta T & Yamaguchi K, *J Chem Phys*, 122 (2005) 114315.
15 Yanai T, Tew D P & Handy N C, *Chem Phys Lett*, 393 (2004) 51.
16 Menezes A P, Jayarama A & Ng S W, *J Cryst Growth*, 402 (2014) 130.

17  Varsanyi G, *Assignments for vibrational spectra of seven hundred benzene derivations*, 1 (Adam Hilger: London), 1974.

18  Roeges N P G, *A guide to the complete interpretation of infrared spectra of organic structures*, (Wiley: New York), 1994.

19  Socrates G, *Infrared and Raman characteristic group frequencies, table and charts*, 3rd Edn, (Wiley: Chichester), 2001.

20  Colthup N B, Daly L H & Wiberley S E, *Introduction to infrared and raman spectroscopy*, (Academic Press: New York), 1990.

21  Politzer P, Murray J S, Lipkowitz K B & Boyd D B, *Molecular electrostatic potentials and chemical reactivity,* (VCH: New York), 1991.

22  Parr R G & Pearson R G, *J Am Chem Soc*, 105 (1983) 7512.

23  Anitha K, Balachandran V & Narayana B, *Int J Curr Res Acta Rev*, 3 (2015) 70.

24  Roy R K, *J Phys Chem A,* 107 (2003) 397.

25  Yang W & Mortier W J, *J Am Chem Soc*, 108 (1986) 5708.

26  Reed A E, Curtiss L A & Weinhold F, *Chem Rev*, 88 (1988) 899.

27  Boyle N M, Tenderholt A L & Langner K M, *J Comput Chem*, 29 (2008) 839.

28  Garza A J, Scuseria G E, Khan S B & Asiri A M, *Chem Phys Lett*, 575 (2013) 122.

29  Anitha K & Balachandran V, *Spectrochim Acta Part A*, 146 (2015) 66.

30  Wang W Y, Du X F, Ma N N, Sun S L & Qiu Y Q, *J Mol Model*, 19 (2013) 1779.

31  Mennuccia B, Cammi R, Cossi M & Tomasi J, *J Mol Struct*, 426 (1998) 191.

32  Ravikumar C, Hubert J I & Jayakumar V S, *Chem Phys Lett*, 460 (2008) 552.

33  Li Y, Li Z R, Wu D, Li R Y, Hao X Y & Sun C C, *J Phys Chem B*, 108 (2004) 3145.